Article

Analysis and Comparison of the Corrosive Behavior of Nickel-Based and Cobalt-Based Dental Alloys

Carmen Marina Garcia-Falcon [1], **Tomas Gil-Lopez** [2,*] , **Amparo Verdu-Vazquez** [2] **and Julia Claudia Mirza-Rosca** [1]

[1] Nanoscience and Nanomaterials, Department of Mechanical Engineering, University of Las Palmas de Gran Canaria, 35017 Las Palmas, Spain; carmen.garcia110@alu.ulpgc.es (C.M.G.-F.); julia.mirza@ulpgc.es (J.C.M.-R.)

[2] Science and Engineering, Department of Building Technology, Madrid Polytechnic University, 28040 Madrid, Spain; amparo.verdu@upm.es

[*] Correspondence: tomas.gill@upm.es

Abstract: Nickel-based and cobalt-based metal alloys are frequently used in dentistry. The introduction of various elements in the alloy changes its characteristics, and a thorough study of each alloy should be completed to determine its appropriate corrosion resistance and biocompatibility in contact with physiological fluids. There are scarce investigations on these widely used dental alloys in Ringer solution, and findings in this research bring new experimental data and information. The present study evaluated and compared the corrosion behavior of six NiCr- and two CoCr-based dental materials in Ringer solution, using the following techniques: potentiostatic polarization curves (chronoamperometry), microstructural analysis, and EIS (electrochemical impedance spectroscopy). The results obtained in this investigation showed that in the NiCr-based specimens Ni4, Ni5, and Ni6 the stability of the passive layer was destroyed after polarization and a development and growth of stable pits was found in the microstructural analysis after electrochemical treatment. In terms of susceptibility to corrosion, two different groups of specimens were derived from this investigation. A first group which included the two CoCr (Co1 and Co2) and three of the six NiCr alloys studied (Ni1, Ni2, and Ni3). A second group with the other NiCr alloys investigated Ni4, Ni5, and Ni6.

Keywords: metal alloys; NiCr; CoCr; electrochemical characterization; corrosion; Ringer solution

1. Introduction

Nickel-based and cobalt-based metal alloys are frequently used in dentistry for prosthodontic restorations due to their advantageous characteristics [1–8]. Nickel in an alloy can cause allergic reactions and toxicity, according to some studies [9–13], but others report very different results and conclusions [14–16]. Furthermore, the introduction of chromium in their composition favors the stability of the alloy in order to be used as biomaterial [17,18]. According to several investigations, the chromium's percentage found in the alloy is a decisive factor in the formation of the passive layer and the resistance to corrosion [19–21]. Cobalt-based alloys are frequently used biomaterials with applications in the dental and cardiac fields, as well as in orthopedic implants [22,23], due to the considerable wear and corrosion resistance properties given by this metallic element [24,25]. As dental materials, they are used for crowns with porcelain fused to metal [26–30], in fixed and removable dental prostheses [31–35], orthodontic wire leads [36,37], oral implants [38–40], and are very suitable in patients whose exposure to nickel might cause an allergic reaction [41,42].

The introduction of other elements in the alloy varies its characteristics. Aluminum, iron, copper, manganese, molybdenum, niobium, silicon, and tungsten can be found on different Ni- and Co-based alloys. As an example, it has been reported that the molybdenum content increases the corrosion resistance of the alloys [20,21] and their appropriateness to

be used in the human body [19] as a biomaterial. Therefore, a thorough study of each alloy should be completed in order to determine its corrosion resistance and biocompatibility. Current research is focused on the investigation of materials to be used in the human body [43].

The alloys studied in this investigation, whether nickel- or cobalt-based, all had chromium in their composition, which makes them supposedly stable and safe to be used as dental alloys and are found in world markets for prosthodontic restorations. However, not all alloys have the same biocompatibility in contact with physiological fluids. The resistance to corrosion is the most important factor to be taken into account, because due to the corrosion process, elements are released into the oral cavity, causing problems that make biological safety difficult [44,45]. Certainly, materials in contact with human tissue must be non-toxic and not cause allergies or inflammations to be biocompatible [46].

Accordingly, in order to safely use these NiCr and CoCr alloys, a thorough analysis must be performed regarding their corrosion behavior. Electrochemical studies for a limited number of NiCr and CoCr alloys in artificial saliva medium were conducted by our group [47–49], and we are now investigating in simulated body fluid (Ringer solution). We have recently presented our study of CoCr alloys [50], but there are scarce investigations on these widely used materials in Ringer solution, and further studies are imperative to analyze and compare these alloys. Findings in this research bring new experimental data and information on these worldwide used NiCr and CoCr dental alloys in simulated body fluid. The present study evaluated and compared the corrosion behavior of six NiCr and two CoCr dental materials in Ringer solution, using microstructural analysis, potentiostatic polarization curves (chronoamperometry), and EIS techniques.

2. Materials and Methods

2.1. Materials, Specimens Preparation

Six NiCr and two CoCr dental alloys commercially used for prosthodontic restorations were studied: three manufactured in Germany, two in Romania, and three in the United States. The dental materials will hereinafter be referred to as specimens Ni1–6 and Co1,2.

The compositions of the eight investigated dental materials are shown in Tables 1 and 2.

The specimens were cut to 1 cm^2 size and each was inserted into an epoxy resin disk. Then, the samples were mechanically abraded using emery paper up to 2500 grit and polished with a 1 μm suspension of alumina. Before testing, the specimens used were cleaned completely in ethyl alcohol and deionized water.

The Ringer solution used as corrosion medium in this investigation had the following composition: NaCl—6.8 g/L, KCl—0.4 g/L, CaCl2—0.2 g/L, NaCO$_3$H—1 g/L, glucose—1 g/L, MgSO$_4$·7H$_2$O—0.2 g/L and NaH$_2$PO$_4$·H$_2$O—0.14 g/L.

Table 1. NiCr dental material composition.

Composition (in wt.%)	Specimens					
	Ni1	Ni2	Ni3	Ni4	Ni5	Ni6
Ni	60.1	60.8	63.4	72.1	64.9	53.4
Cr	24.3	23.9	23.2	20	17.9	14.4
Mo	10.1	8.8	3			
Fe	2.1	2.4	9	7.5		
Nb	1	3.8				
Si				1	1.8	1.5
Cu					9.9	9.5
Mn		2			3.6	19.4
Al					1.5	1.6

Table 2. CoCr dental material composition.

Composition (in wt.%)	Specimens	
	Co1	Co2
Co	63.5	63.4
Cr	27	29.0
Mo	5.5	5.2
Fe	2	
Ni	1	

2.2. Microstructural Characterization

To study the microstructure of the six NiCr- and two CoCr-based dental materials, a chemical reactant containing 10 mL HNO_3, 30 mL HCl and 20 mL glycerine [51] and an PME 3-ADL microscope (Olympus, Tokyo, Japan), were utilized in the investigation. After electrochemical treatment, an analysis of the surface modifications of the NiCr and CoCr alloys using the microscope was conducted.

2.3. Electrochemical Measurements

The analysis was conducted in a three-electrode electrochemical cell, using as a reference electrode a saturated calomel electrode (or SCE), a platinum auxiliary electrode, and the sample as working electrode. A Princeton Applied Research (PAR, Oak Ridge, TN, USA) model 263A potentiostat, a lock-in amplifier 5210 (PAR, Oak Ridge, TN, USA), and a computer with Electrochemistry Power Suite software (PAR, Oak Ridge, TN, USA) were used.

2.3.1. Potentiostatic Polarization Studies—Chronoamperometry

Chronoamperometry measurements were performed at a potential of 0.1 V/ESC on the working electrode. Using the electrochemical chronoamperometry technique, the induction time could be determined prior to the increase in the current density due to the breakdown of the passive layer. The current density variations of each of the different NiCr and CoCr dental alloys polarized at +100 mV/ESC in Ringer solution for 5 h were analyzed in this research. All tests were performed three times, and data acquisition and processing was performed with PowerCorr Princeton Applied Research software (PAR, Oak Ridge, TN, USA). After the potentiostatic polarization tests, the microstructures of the alloys' surfaces were examined with the ADL microscope OLYMPUS PME3 (Olympus, Tokyo, Japan).

2.3.2. EIS—Electrochemical Impedance Spectroscopy

EIS tests of the eight NiCr- and CoCr-based alloys were conducted for analysis and comparison of the corrosion resistance in Ringer solution following the potentiostatic polarization studies. The EIS spectra were recorded at the 100 mV/ESC potential after plotting the potentiostatic curves for 5 h.

Experimental EIS results were analyzed with ZSimpWin Princeton Applied Research software (PAR, Oak Ridge, TN, USA) to obtain the equivalent circuit (EC) where experimental data and simulated responses fitted well. Following each experiment, impedance data were displayed as Nyquist plots, Bode |Z|, and Bode phase diagrams. All tests were performed three times.

3. Results and Discussions

The potentiostatic polarization curves (chronoamperometry) for NiCr alloys in Ringer solution at a potential of 100 mV/ESC are shown in Figure 1.
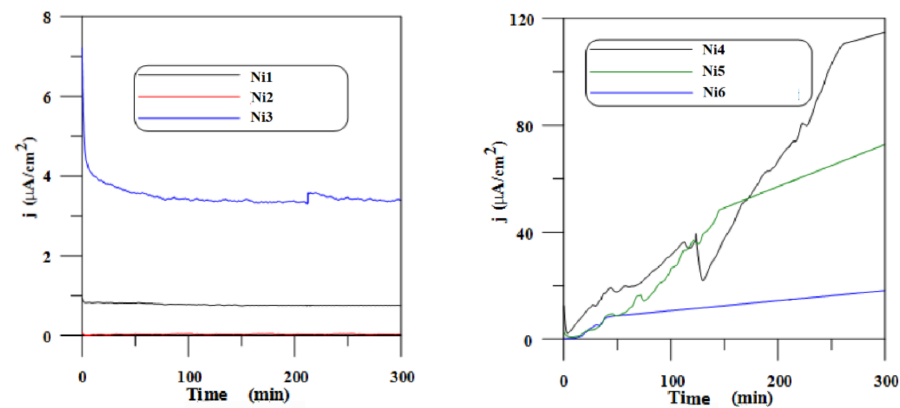
Figure 1. Potentiostatic polarization curves for specimens Ni1, Ni2, Ni3, Ni4, Ni5, and Ni6 in Ringer solution at a potential of 100 mV/ESC.

In human organisms, pure titanium may be exposed to a maximum potential of about 450 or 550 mV/ESC [52]. For Co–Cr–Mo biomaterials, this information could not be found. Nevertheless, for physiological conditions in the human body, a metallic biomaterial's potential value may fluctuate between −1.0 and 1.2 V, according to Black's diagram of the potential pH [53].

In these conditions, it was found for some tested materials with very low potentials, that the stability of the passive layer in human organisms may be achieved at +100 mV/ESC. For this purpose, the potentiostatic polarization curves were plotted at a potential of +100 mV/ESC for 5 h, to prove the stability of the passive layer at this potential of +100 mV/ESC potentially achievable in the human body.

In the case of NiCr-based dental alloys, the polarization current of specimens Ni1, Ni2, and Ni3 at 100 mV/ESC in Ringer solution oscillated around 0.8 $\mu A/cm^2$, 0.2 $\mu A/cm^2$, and 3.8 $\mu A/cm^2$, respectively. Specimens Ni4, Ni5, and Ni6 showed an increase in current density, higher in the cases of specimens Ni4 and Ni5.

Microstructures of specimens Ni1, Ni2, and Ni3 after the 5 h potentiostatic treatment are shown in Figure 2. No degradation was observed in these specimens after the 5 h potentiostatic treatment.
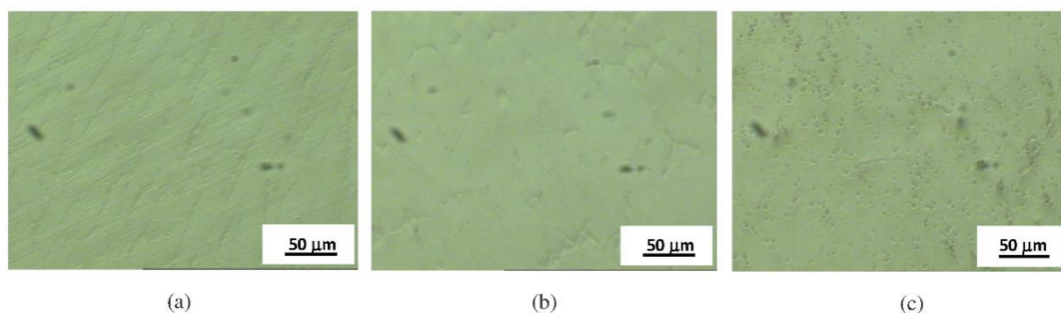

Figure 2. Microstructures after electrochemical treatment for (**a**) specimen Ni3, (**b**) specimen Ni1, and (**c**) specimen Ni2.

For specimens Ni4, Ni5, and Ni6 the increase in current density is probably caused by the active anodic dissolution of the surface due to the film breakdown, with the formation and growth of stable pits. In Figure 3, microstructures of specimens Ni4, Ni5, and Ni6 before and after electrochemical treatments are presented.
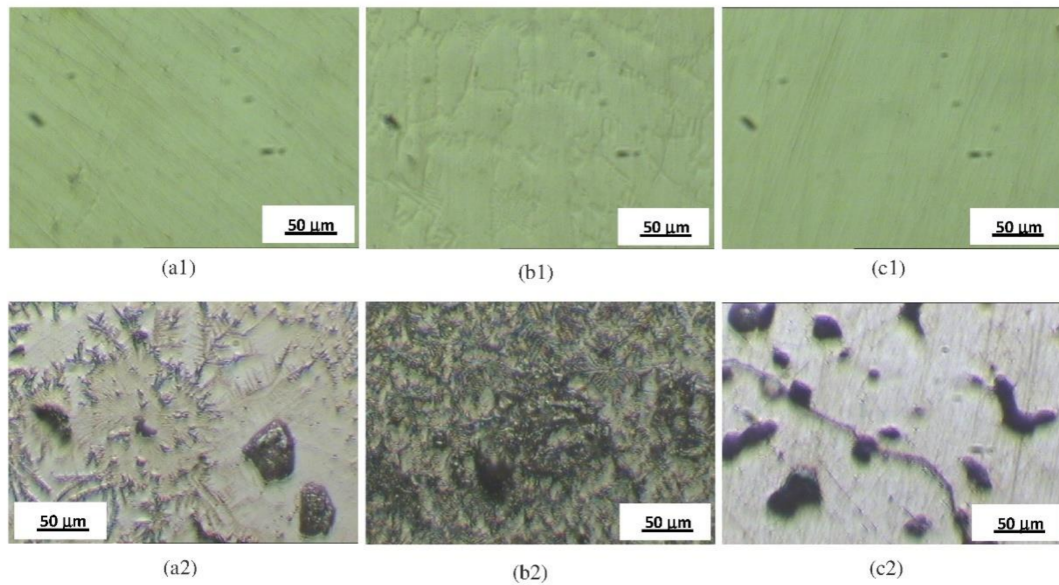
Figure 3. Microstructures before electrochemical treatments for (**a1**) specimen Ni5, (**b1**) specimen Ni4, (**c1**) specimen Ni6; after electrochemical treatments for (**a2**) specimen Ni5, (**b2**) specimen Ni4, and (**c2**) specimen Ni6.

The potentiostatic polarization curves for CoCr alloys in Ringer solution at a potential of 100 mV/ESC are displayed in Figure 4.
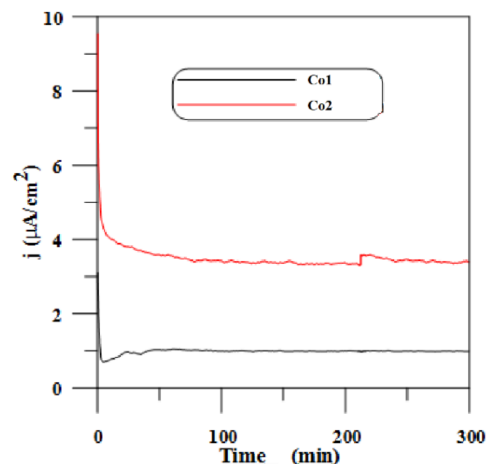

Figure 4. The potentiostatic polarization curves for specimens Co1 and Co2 in Ringer solution at a potential of 100 mV/ESC.

The polarization current of specimens Co1 and Co2 at 100 mV/SCE in Ringer solution fluctuated around 1 $\mu A/cm^2$ and 4 $\mu A/cm^2$, respectively.

Microstructures of specimens Co1 and Co2 after 5 h of potentiostatic treatment are shown in Figure 5. No degradation was observed in the CoCr-based dental alloys studied after the 5 h potentiostatic treatment.

After plotting the potentiostatic curves for 5 h, EIS spectra were recorded at the same potential of 100 mV/ESC. Representative results of Bode spectra and Nyquist plot diagrams for the NiCr-based dental alloys, polarized at 100 mV/ESC in Ringer solution, are shown in Figure 6.
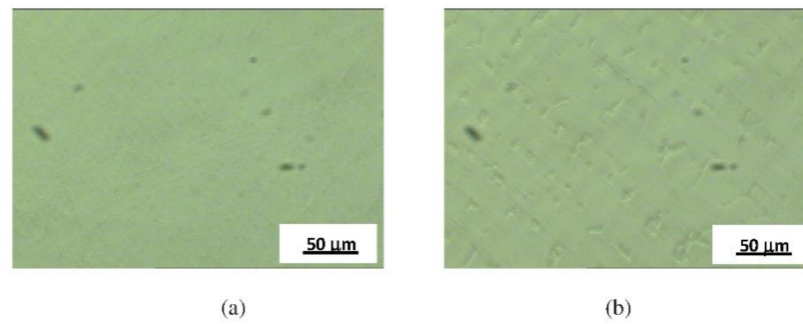
Figure 5. Microstructures after electrochemical treatments for (**a**) specimen Co2 and (**b**) specimen Co1.

Figure 6. Bode spectra and Nyquist plot diagrams for NiCr-based dental alloys in Ringer solution at a potential of 100 mV/ESC. (**A**) Specimen Ni1. (**B**) Specimen Ni2. (**C**) Specimen Ni3. (**D**) Specimen Ni4. (**E**) Specimen Ni6. (**F**) Specimen Ni5.

Representative results of Bode spectra and Nyquist plot diagrams for the studied CoCr-based dental alloys, polarized at 100 mV/ESC in Ringer solution, are shown in Figure 7.
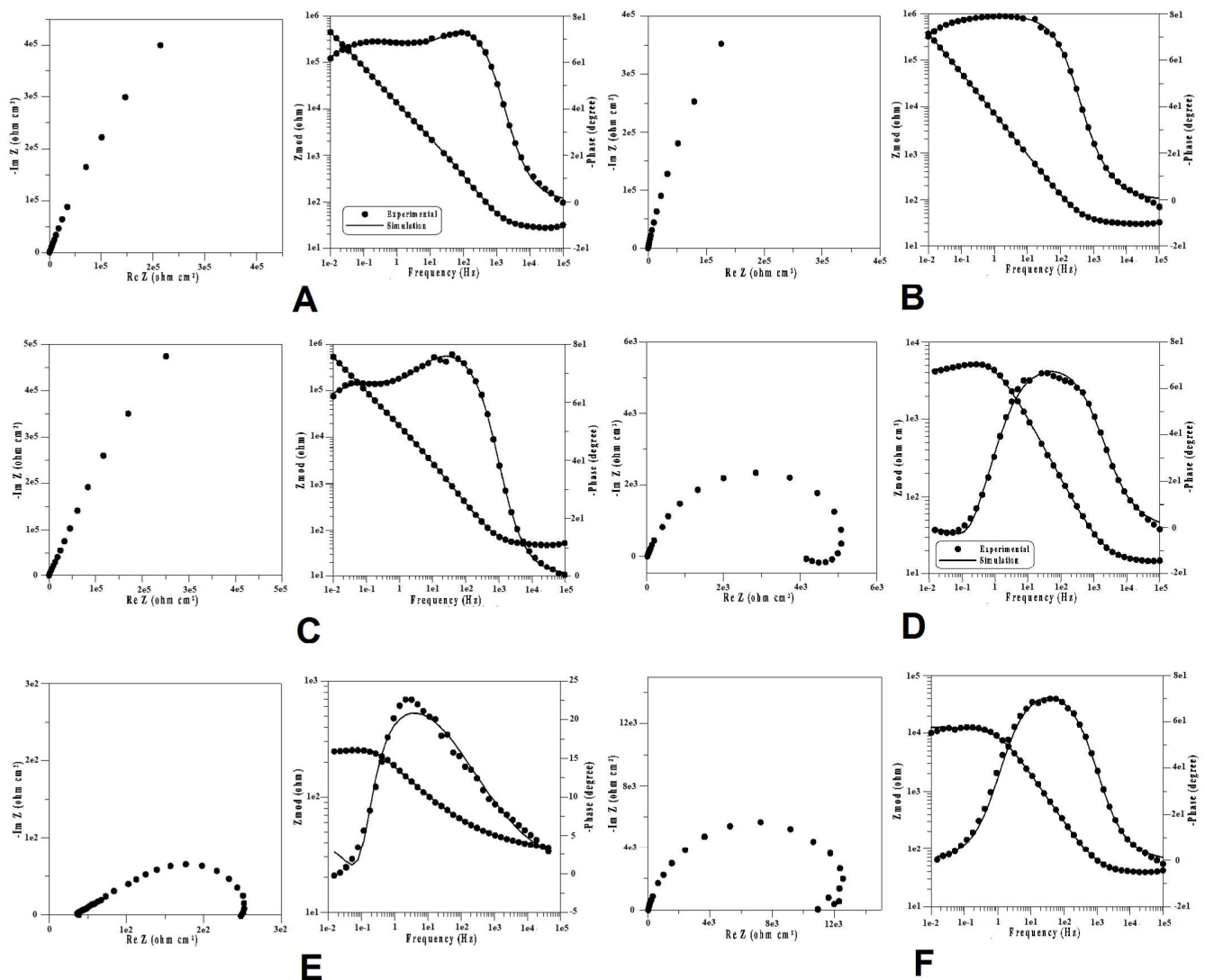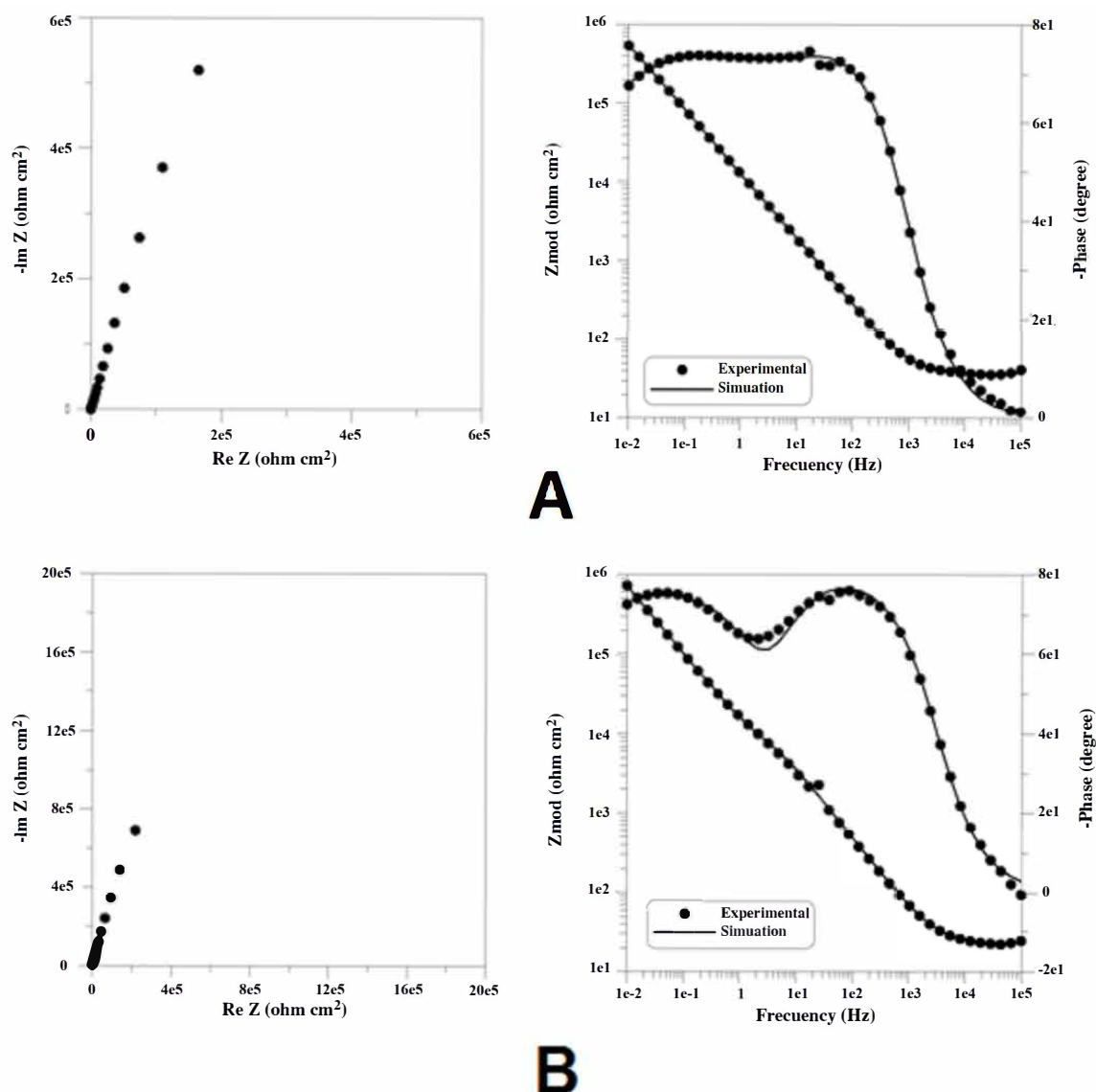
Figure 7. Bode spectra and Nyquist plot diagrams for CoCr-based dental alloys in Ringer solution at a potential of 100 mV/ESC. (**A**) Specimen Co1. (**B**) Specimen Co2.

The experimental measurements are presented in the diagrams as distinct points, and the theoretical spectra that resulted from the equivalent circuit model used are displayed as lines.

The Nyquist spectrum showed that all alloys had a capacitive behavior with the immersion time in Ringer solution, except specimens Ni4, Ni5, and Ni6, which showed an inductive arc. In the electrochemical system, this arc can be associated with the process of metallic dissolution, showing values that are negative for the imaginary impedance [54].

An equivalent circuit, EC, gives the most notable corrosion indicators that can be applied to the substrate–electrolyte system and is formed by a group of different capacitors, resistances, and other circuit components. It is essential to have a proper model of the electrochemical reactions taking place at the electrodes to be able to interpret the system's electrochemical behavior from EIS spectra. An EC representing an electrochemical cell displays impedance to a small sinusoidal excitation.

Starting with the easiest one, several models of electrical circuits were examined when analyzing the impedance data [28,55] for specimens Ni1, Ni2, Ni3, Co1, and Co2, with the best fit obtained for all the determinations using the EC presented in Figure 8.
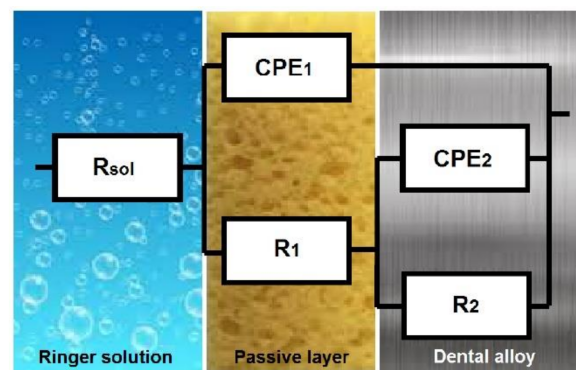
Figure 8. EC used to generate the simulated data for specimens Ni1, Ni2, Ni3, Co1, and Co2.

In the model presented in Figure 8, the ohmic resistance of the electrolyte was designated R_{sol}, the resistance of the passive film was designated R1, the passive film capacitance was represented as CPE_1, the charge transfer resistance (R_{ct}) was designated R_2, and the double-layer capacitance was represented as CPE_2. The EC model was very similar to that from M. Meticos-Hukovic et al. [56] for CoCr alloys dipped in Hank's solution. As a result of the heterogeneous and thin oxide layer formed on the surface of the metallic alloys and the noticeable Bode plots' deviations, it was necessary to substitute the "ideal" capacitance with a constant phase element (CPE), for which impedance is given by $Z = (j\omega)-nY_0$, where j is an imaginary number ($j^2 = -1$), ω is the angular frequency ($rad \cdot s^{-1}$), Y_0 is the constant of CPE ($Scm^{-2}s^n$), n is the power number indicating the deviation from ideal behavior, $n = \alpha(\pi/2)$, and α is the constant phase angle of the CPE (rad).

The main parameters of the EC model for specimens Ni1, Ni2, Ni3, Co1, and Co2 are shown in Table 3. These parameters had the same meaning for all the alloys studied. The value around 10^{-4} from the χ^2 or chi-squared distribution test proves that it was correct to use the constant phase element in the EC model, and also indicated a very good correspondence of fitted values and experimental data.

Table 3. Main parameters of the EC used for specimens Ni1, Ni2, Ni3, Co1, and Co2.

Specimens	R_{sol} $\Omega\,cm^2$	R_1 $\Omega\,cm^2$	Y_{01} $Scm^{-2}s^n$	n_1	R_2 $\Omega\,cm^2$	Y_{02} $Scm^{-2}s^n$	n_2	χ^2
Ni1	28	5×10^3	8.9×10^{-6}	0.83	5.5×10^5	9.7×10^{-6}	0.8	2×10^{-4}
Ni2	35	3×10^3	1.9×10^{-5}	0.9	6.2×10^5	1×10^{-5}	0.88	4×10^{-4}
Ni3	49	1.5×10^4	8.4×10^{-6}	0.89	5.9×10^5	7.1×10^{-6}	0.82	5×10^{-4}
Co1	37	1.5×10^4	7.8×10^{-6}	0.9	9.1×10^5	8.3×10^{-6}	0.83	2×10^{-4}
Co2	55	1.4×10^4	6.1×10^{-6}	0.9	1.2×10^6	8.6×10^{-6}	0.83	6×10^{-4}

In the case of specimens Ni4, Ni5, and Ni6 polarized for 5 h in Ringer solution at a potential of 100 mV/ESC, the best simulations were performed using the equivalent circuit exhibited in Figure 9; the main parameters are shown in Table 4.

As previously stated, the value of around 10^{-4} from the χ^2, or chi-squared distribution test, proved that it was correct to use the constant phase element in the EC model, and indicated an outstanding correspondence of fitted values and experimental data.
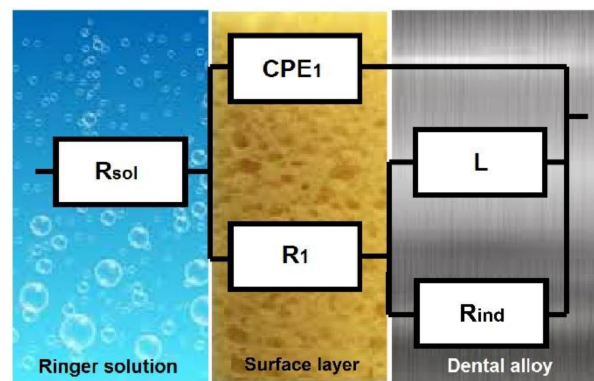
Figure 9. EC used to generate the simulated data for specimens Ni4, Ni5, and Ni6.

Table 4. Main parameters of the EC used for specimens Ni4, Ni5, and Ni6.

Specimens	R_{sol} Ω cm^2	R_1 Ω cm^2	Y_{01} Scm^{-2}s^n	n_1	R_{ind} Ω cm^2	L Henri cm^2	χ^2
Ni4	20	4.5×10^3	3.1×10^5	0.8	1.7×10^3	1.4×10^3	8×10^{-4}
Ni5	38	1.1×10^4	1.5×10^{-5}	0.84	9×10^2	3×10^3	6×10^{-4}
Ni6	34	260	$2.4\ 10^{-3}$	0.4	240	231	6×10^{-4}

In the model exhibited in Figure 9, the ohmic resistance of the electrolyte was designated R_{sol}, and the surface film resistance and capacitance were designated R_1 and CPE_1, respectively. It was found that the presence of an inductive process was characterized by a resistance R_{ind} and an inductance L, associated with an adsorption–desorption process that occurred in the formation of the surface film.

For this circuit, the total impedance was:

$$Z_{eq} = R_{sol} + \cfrac{1}{jwC_1 + \cfrac{1}{R_1 + \cfrac{1}{\frac{1}{R_{ind}} + \frac{1}{jwL}}}} \tag{1}$$

After standard calculations, the following equation was obtained:

$$Z_{eq} = R_{sol} + \frac{R - w^2RT + w^2AB}{\left(1 - w^2T\right)^2 + w^2R^2} + jw\frac{B - RA - w^2TB}{\left(1 - w^2T\right)^2 + w^2A^2} \tag{2}$$

where $R = R_1 + R_{ind}$, $T = \tau_1\,\tau_2$, $A = \tau_1 + \tau_2 + C_1\,R_{ind}$, $B = \tau_2\,R_1$, $\tau_1 \equiv$ time constant of process at passive layer [s], and $\tau_2 \equiv$ time constant of inductive process [s].

The equivalent circuit has a physical meaning associated with the passive layer itself, R_2CPE_2, and the passive layer/electrolyte interface, R_1CPE_1. The passive film was not destroyed by polarization at 100 mV/ESC for the two CoCr-based alloys (Co1 and Co2) or the NiCr-based alloys Ni1, Ni2, and Ni3. This fact was confirmed by potentiostatic polarization curves and surface microscopy after polarization.

From the data presented in Table 3, it was found that the stability of the materials was high at this potential due to the polarization resistance, which had high values compared to those obtained after one week of immersion in Ringer solution (greater than 10^5 Ω cm^2). The most stable alloy at the 100 mV/ESC potential was one based on CoCr, specimen Co2. Its polarization resistance of 10^6 Ω cm^2, according to different studies and the ASM Handbook [57–60], is characteristic of alloys with very high corrosion resistance.

The resultant parameters of the equivalent circuit, for the other three NiCr alloys, are presented in Table 4. Results showed that after polarization at 100 mV/ESC, the passive layer was destroyed (the inductance L is associated with the film dissolution).

When specimens Ni4, Ni5, and Ni6 were polarized at 100 mV/ESC, the passive layer developed on these alloys was considerably destroyed, and the impedance of the alloys was related to the R_{ct} or charge transfer resistance. As a result, there was no protective passive layer.

Additionally, it was observed that out of the three alloys, depending on the value of the polarization resistance ($R_p = R_1 + R_{ind}$), the highest stability was presented by specimen Ni5 and the lowest by specimen Ni6. A comparison with the polarization resistance values obtained after 7 days of immersion in Ringer solution revealed decreases of approximately 70-fold in the case of specimen Ni5, nearly 100-fold in the case of specimen Ni4, and about 500-fold for Specimen Ni6.

4. Conclusions

This investigation evaluated and compared the corrosive behavior of six NiCr- and two CoCr-based dental alloys in Ringer's solution. Using potentiostatic polarization curves (chronoamperometry), microstructural analysis, and EIS, the following conclusions were derived:

1. The stability of the passive layer was not destroyed for the CoCr-based specimens Co1 and Co2, or the NiCr-based specimens Ni1, Ni2, and Ni3. This fact was confirmed by potentiostatic polarization curves and surface microscopy after polarization;
2. In the cases of specimens Ni4, Ni5, and Ni6, it was found that the passive layer was destroyed after polarization. Therefore, there was no longer a protective passive layer on these alloys;
3. Findings from the micrographs of the different NiCr and CoCr dental alloys studied after electrochemical treatments showed that there was no degradation for specimens Ni1, Ni2, Ni3, Co1, and Co2, but the development and growth of stable pits was discovered on the surfaces of specimens Ni4, Ni5, and Ni6;
4. According to the results obtained, in terms of susceptibility to corrosion from the spectral data, the NiCr and CoCr dental alloys were divided in two different groups. A first group which included the two CoCr (Co1 and Co2) and three of the six NiCr alloys studied (Ni1, Ni2, and Ni3), where the polarization resistance showed high values. In this group, the most stable alloy was specimen Co2, with a polarization resistance in the order of $10^6 \ \Omega \ cm^2$, characteristic of alloys highly resistant to corrosion. A second group with the other NiCr alloys investigated, Ni4, Ni5, and Ni6, where the passive layers were destroyed after polarization and the polarization resistance determinations were significantly lower than those exhibited by the first group. In this second group, specimen Ni5 had the highest stability and specimen Ni6 the lowest, based on polarization resistance values.

Author Contributions: Conceptualization, C.M.G.-F.; Writing—original draft, C.M.G.-F.; Methodology, C.M.G.-F. and T.G.-L.; Investigation, C.M.G.-F. and T.G.-L.; Validation, T.G.-L.; Formal analysis, C.M.G.-F. and T.G.-L.; Data curation, T.G.-L. and A.V.-V.; Writing—review and editing, A.V.-V.; Software, J.C.M.-R.; Supervision, J.C.M.-R. All authors have read and agreed to the published version of the manuscript.

Institutional Review Board Statement: Not applicable.

Informed Consent Statement: Not applicable.

Data Availability Statement: The data presented in this study are available on request from the corresponding author.

Conflicts of Interest: The authors declare no conflict of interest.

References

1. Warlimont, H. Nickel and Nickel Alloys. In *Springer Handbook of Materials Data*; Warlimont, H., Martienssen, W., Eds.; Springer International Publishing: Cham, Switzerland, 2018.
2. Moris, I.; Sakuma, M.; Faria, A.; Macedo, A.; Ribeiro, R.; Rodrigues, R. The dental alloys determine the choice of composite resins to be used. *Braz. Dent. Sci.* **2017**, *20*, 92–98. [CrossRef]
3. Cha, M.S.; Huh, Y.H.; Cho, L.R.; Park, C.J. A comparative study of the wear of dental alloys against monolithic zirconia. *J. Prosthet. Dent.* **2020**, *123*, 866–873. [CrossRef]
4. Chen, Q.; Thouas, G.A. Metallic implant biomaterials. *Mater. Sci. Eng. R* **2015**, *87*, 1–57. [CrossRef]
5. Torabinejad, V.; Aliofkhazraei, M.; Assareh, S.; Allahyarzadeh, M.H.; SabourRouhaghdam, A. Electrodeposition of Ni-Fe alloys, composites, and nano coatings—A review. *J. Alloys Compd.* **2017**, *691*, 841–859. [CrossRef]
6. Musa, A.Y.; Behazin, M.; Wren, J.C. Potentiostatic oxide growth kinetics on Ni–Cr and Co–Cr alloys. Potential and pH dependences. *Electrochim. Acta* **2015**, *162*, 185–197. [CrossRef]
7. Kuznetsov, V.V.; Filatova, E.A.; Telezhkina, A.V.; Kruglikov, S.S. Corrosion resistance of Co−Cr−W coatings obtained by electrodeposition. *J. Solid State Electrochem.* **2018**, *22*, 2267–2276. [CrossRef]
8. Chen, Y.; Li, Y.; Kurosu, S.; Meng, Q.; Tang, N.; Koizumi, Y.; Chiba, A. Analysis of in vitro wear behaviour and contact mechanisms of metal-on-metal hip joint bearings with different radial clearances. *Mater. Trans.* **2015**, *56*, 826–834. [CrossRef]
9. Hornez, J.C.; Lefèvre, A.; Joly, D.; Hildebrand, H.F. Multiple parameter cytotoxicity index on dental alloys and pure metals. *Biomol. Eng.* **2002**, *19*, 103–117. [CrossRef]
10. Messer, R.L.; Lucas, L.C. Cytotoxic evaluation of ions released from nickel-chromium dental alloys. *J. Dent. Res.* **1996**, *75*, 255.
11. Messer, R.L.; Lucas, L.C. Evaluation of metabolic activities as biocompatibility tools: A study of individual ions' effects on fibroblasts. *Dent. Mater.* **1999**, *15*, 1–6. [CrossRef]
12. Elshahawy, W.M.; Watanabe, I.; Kramer, P. In vitro cytotoxicity evaluation of elemental ions released from different prosthodontic materials. *Dent. Mater.* **2009**, *25*, 1551–1555. [CrossRef]
13. Nelson, S.K.; Wataha, J.C.; Lockwood, P.E. Accelerated toxicity testing of casting alloys and reduction of intraoral release of elements. *J. Prosthet. Dent.* **1999**, *81*, 715–720. [CrossRef]
14. Alp, G.; Çakmak, G.; Sert, M.; Burgaz, Y. Corrosion potential in artificial saliva and possible genotoxic and cytotoxic damage in buccal epithelial cells of patients who underwent Ni-Cr based porcelain-fused-to-metal fixed dental prostheses. *Mutat. Res. Genet. Toxicol. Environ. Mutagen* **2018**, *827*, 19–26. [CrossRef] [PubMed]
15. Craig, R.G.; Hanks, C.T. Reaction of fibroblasts to various dental casting alloys. *J. Oral Pathol.* **1988**, *17*, 341–347. [CrossRef] [PubMed]
16. Craig, R.G.; Hanks, C.T. Cytotoxicity of experimental casting alloys evaluated by cell culture tests. *J. Dent. Res.* **1990**, *69*, 1539–1542. [CrossRef]
17. Friend, W.Z. *Corrosion of Nickel and Nickel-Based Alloys*; John Wiley and Sons: New York, NY, USA, 1980.
18. Wylie, C.M.; Shelton, R.M.; Fleming, G.J.P.; Davenport, A.J. Corrosion of nickel-based dental casting alloys. *Dent. Mater.* **2007**, *23*, 714–723. [CrossRef] [PubMed]
19. Moslehifard, E.; Ghasemzadeh, S.; Nasirpouri, F. Influence of pH level of artificial saliva on corrosion behavior and nickel ion release of a Ni-Cr-Mo alloy: An in vitro study. *Anti-Corros. Methods Mater.* **2019**, *66*, 746–756. [CrossRef]
20. Pan, Y.; Lin, Y.; Jiang, L.; Lin, H.; Xu, C.; Lin, D.; Cheng, H. Removal of dental alloys and titanium attenuates trace metals and biological effects on liver and kidney. *Chemosphere* **2020**, *243*, 125205. [CrossRef]
21. Rodrigues, W.C.; Broilo, L.R.; Schaeffer, L.; Knörnschild, G.; Espinoza, F.R.M. Powder metallurgical processing of Co–28%Cr–6%Mo for dental implants: Physical, mechanical and electrochemical properties. *Powder Technol.* **2011**, *206*, 233–238. [CrossRef]
22. Xiao, M.; Chen, Y.M.; Biao, M.N.; Zhang, X.D.; Yang, B.C. Bio-functionalization of biomedical metals. *Mater. Sci. Eng. C* **2017**, *70 Pt 2*, 1057–1070. [CrossRef]
23. Gurappa, I. Development of appropriate thickness ceramic coatings on 316 L stainless steel for biomedical applications. *Surf. Coat. Technol.* **2002**, *161*, 70–78. [CrossRef]
24. Hamidi, M.F.F.A.; Harun, W.S.W.; Samykano, M.; Ghani, S.A.C.; Ghazalli, Z.; Ahmadd, F.; Sulong, A.B. A review of biocompatible metal injection moulding process parameters for biomedical applications. *Mater. Sci. Eng. C* **2017**, *78*, 1263–1276. [CrossRef]
25. Chen, Y.; Li, Y.; Kurosu, S.; Yamanaka, K.; Tang, N.; Chiba, A. Effects of microstructures on the sliding behavior of hot-pressed CoCrMo alloys. *Wear* **2014**, *319*, 200–210. [CrossRef]
26. Chenakin, S.P.; Filatova, V.S.; Makeeva, I.N.; Vasylyev, M.A. Ultrasonic impact treatment of CoCrMo alloy: Surface composition and properties. *Appl. Surf. Sci.* **2017**, *408*, 11–20. [CrossRef]
27. Gong, X.; Li, Y.; Nie, Y.; Huang, Z.; Liu, F.; Huang, L.; Jiang, L.; Mei, H. Corrosion behaviour of CoCrMo alloy fabricated by electron beam melting. *Corros. Sci.* **2018**, *139*, 68–75. [CrossRef]
28. Qian, C.; Wu, X.; Zhang, F.; Yu, W. Electrochemical impedance investigation of Ni-free Co-Cr-Mo and Co-Cr-Mo-Ni dental casting alloy for partial removable dental prosthesis frameworks. *J. Prosthet. Dent.* **2016**, *116*, 112–118. [CrossRef]
29. Henriques, B.; Bagheri, A.; Gasik, M.; Souza, J.C.M.; Carvalho, O.; Silva, F.S.; Nascimento, R.M. Mechanical properties of hot pressed CoCrMo alloy compacts for biomedical applications. *Mater. Design* **2015**, *83*, 829–834. [CrossRef]
30. Park, W.U.; Park, H.G.; Hwang, K.H.; Zhao, J.; Lee, J.K. Interfacial Property of Dental Cobalt–Chromium Alloys and Their Bonding Strength with Porcelains. *J. Nanosci. Nanotechnol.* **2017**, *17*, 2585–2588. [CrossRef]

31. Ramírez-Ledesma, A.L.; Roncagliolo, P.; Álvarez-Pérez, M.A.; Lopez, H.F.; Juárez-Islas, J.A. Corrosion Assessment of an Implantable Dental Co-Cr Alloy in Artificial Saliva and Biocompatibility Behavior. *J. Mater. Eng. Perform.* **2020**, *29*, 1657–1670. [CrossRef]

32. Lucchetti, M.C.; Fratto, G.; Valeriani, F.; De Vittori, E.; Giampaoli, S.; Papetti, P.; Spica, V.R.; Manzon, L. Cobalt-chromium alloys in dentistry: An evaluation of metal ion release. *J. Prosthet. Dent.* **2015**, *114*, 602–608. [CrossRef] [PubMed]

33. de Freitas, B.X.; Nunes, C.A.; dos Santos, C. Sintering behaviour of Co-28%Cr-6%Mo compacted blocks for dental prosthesis. *J. Mater. Res. Technol.* **2019**, *8*, 2052–2062. [CrossRef]

34. Alharbi, N.; Wismeijer, D.; Osman, R.B. Additive manufacturing techniques in prosthodontics: Where do we currently stand? A critical review. *Int. J. Prosthodont.* **2017**, *30*, 474–484. [CrossRef] [PubMed]

35. Svanborg, P.; Hjalmarsson, L.A. systematic review on the accuracy of manufacturing techniques for cobalt chromium fixed dental prostheses. *Biomater. Investig. Dent.* **2020**, *7*, 31–40. [CrossRef] [PubMed]

36. Kono, H.; Kikuchi, M. Analysis of orthodontic wire springback to simplify wire bending. *Orthod. Waves* **2020**, *79*, 57–63. [CrossRef]

37. Hanawa, T. *Novel Structured Metallic and Inorganic Materials*; Springer: Singapore, 2019.

38. Park, J.; Lee, H.; Kang, S.; Kim, J.; Kim, J. Effect of core materials for core fabrication for dental implants on in-vitro cytocompatibility of MC3T3-E1 cells. *BMC Oral Health* **2019**, *19*, 284. [CrossRef]

39. Bilgin, M.S.; Erdem, A.; Dilber, E.; Ersoy, İ. Comparison of fracture resistance between cast, CAD/CAM milling, and direct metal laser sintering metal post systems. *J. Prosthodont. Res.* **2016**, *60*, 23–28. [CrossRef]

40. Xia, Y.; Zhao, J.; Dong, Z.; Guo, X.; Tian, Q.; Liu, Y. A Novel Method for Making Co-Cr-Mo Alloy Spherical Powder by Granulation and Sintering. *JOM J. Miner. Met. Mater. Soc.* **2020**, *72*, 1279–1285. [CrossRef]

41. Wataha, J.C.; Messer, R.L. Casting alloys. *Dent. Clin. N. Am.* **2004**, *48*, 499–512. [CrossRef]

42. Roberts, H.W.; Berzins, D.W.; Moore, B.K.; Charlton, D.G. Metal–ceramic alloys in dentistry: A review. *J. Prosthodont.* **2009**, *18*, 188–194. [CrossRef]

43. Yang, Y.; Lu, C.; Shen, L.; Zhao, Z.; Peng, S.; Shuai, C. In-situ deposition of apatite layer to protect Mg-based composite fabricated via laser additive manufacturing. *J. Magnes. Alloy.* 2021; in press. [CrossRef]

44. Vyas, R.; Issaid, M.A.; Idris, B.A. Biocompatibility and corrosive resistance. *Cairo Dent. J.* **2009**, *25*, 361–365.

45. Rupp, F.; Liang, L.; Geis-Gerstorfer, J.; Scheideler, L.; Hüttig, F. Surface characteristics of dental implants. *Dent. Mater.* **2018**, *34*, 40–57. [CrossRef]

46. Manam, N.S.; Harun, W.S.W.; Shri, D.N.A.; Ghani, S.A.C.; Kurniawan, T.; Ismail, M.H.; Ibrahim, M.H.I. Study of corrosion in biocompatible metals for implants: A review. *J. Alloys Compd.* **2017**, *701*, 698–715. [CrossRef]

47. Mareci, D.; Ungureanu, G.; Aelenei, N.; Chelariu, R.; Mirza-Rosca, J.C. EIS diagnosis of some dental alloys in artificial saliva. *Environ. Eng. Manag. J.* **2007**, *6*, 313–317. [CrossRef]

48. Mareci, D.; Ungureanu, G.; Aelenei, N.; Mirza-Rosca, J.C. Comparative corrosion study of non-precious Ni/Cr-based soft alloys in view of dental applications. *Environ. Eng. Manag. J.* **2008**, *7*, 41–49. [CrossRef]

49. Mareci, D.; Sutiman, D.; Cailean, A.; Bolat, G. Comparative corrosion study of Ag-Pd and Co-Cr alloys used in dental applications. *Bull. Mater. Sci.* **2010**, *33*, 491–500. [CrossRef]

50. Garcia-Falcon, C.M.; Gil-Lopez, T.; Verdu-Vazquez, A.; Mirza-Rosca, J.C. Electrochemical characterization of some cobalt base alloys in Ringer solution. *Mater. Chem. Phys.* **2021**, *260*, 124164. [CrossRef]

51. Geru, N.; Bane, M.; Gurgu, C. *Analiza Structurii Materialelor Metalice (The Analysis of the Structure of Metallic Materials)*; Editura Tehnica: Bucharest, Romania, 1991.

52. Rondelli, G.; Vicentini, B. Effect of copper on the localized corrosion resistance of Ni-Ti shape memory alloy. *Biomaterials* **2002**, *23*, 639–644. [CrossRef]

53. Black, J. *Biological Performance of Materials: Fundamentals of Biocompatibility*; CRC Press: Boca Raton, FL, USA, 2006.

54. Newman, R.C.; Mehta, A. An ac impedance study of the de-alloying of Fe Ni alloys, and its relevance to chloride scc of stainless steels. *Corros. Sci.* **1998**, *28*, 1183–1187. [CrossRef]

55. Turdean, G.L.; Craciun, A.; Popa, D.; Constantiniuc, M. Study of electrochemical corrosion of biocompatible Co–Cr and Ni–Cr dental alloys in artificial saliva. Influence of pH of the solution. *Mater. Chem. Phys.* **2019**, *233*, 390–398. [CrossRef]

56. Meticos-Hukovic, M.; Pilic, Z.; Babic, R.; Omanovic, D. Influence of alloying elements on the corrosion stability of CoCrMo implant alloy in Hank's solution. *Acta Biomater.* **2006**, *2*, 693–700. [CrossRef]

57. Vander Voort, G.F. *ASM Handbook Volume 9: Metallography and Microstructures*; ASM International: Materials Park, OH, USA, 2004.

58. Jones, D.A. *Principles and Prevention of Corrosion*; Harlow Pearson Education: Harlow, UK, 2014.

59. Huang, H.H. Electrochemical impedance spectroscopy study of strained titanium in fluoride media. *Electrochim. Acta* **2002**, *47*, 2311–2318. [CrossRef]

60. Pan, J.; Thierry, D.; Leygraf, C. Electrochemical impedance spectroscopy study of the passive oxide film on titanium for implant application. *Electrochim. Acta* **1996**, *41*, 1143–1153. [CrossRef]